Spectral and total temperature-dependent emissivities of few-layer structures on a metallic substrate

Etienne Blandre,* Pierre-Olivier Chapuis, and Rodolphe Vaillon

Université de Lyon, CNRS, INSA-Lyon, UCBL, CETHIL, UMR5008, F-69621, Villeurbanne, France

*etienne.blandre@insa-lyon.fr

Abstract: We investigate the thermal radiative emission of few-layer structures deposited on a metallic substrate and its dependence on temperature with the Fluctuational Electrodynamics approach. We highlight the impact of the variations of the optical properties of metallic layers on their temperature-dependent emissivity. Fabry-Pérot spectral selection involving at most two transparent layers and one thin reflective layer leads to well-defined peaks and to the amplification of the substrate emission. For a single Fabry-Pérot layer on a reflective substrate, an optimal thickness that maximizes the emissivity of the structure can be determined at each temperature. A thin lossy layer deposited on the previous structure can enhance interference phenomena, and the analysis of the participation of each layer to the emission shows that the thin layer is the main source of emission. Eventually, we investigate a system with two Fabry-Pérot layers and a metallic thin layer, and we show that an optimal architecture can be found. The total hemispherical emissivity can be increased by one order of magnitude compared to the substrate emissivity.

OCIS codes: (030.5620) Radiative transfer; (310.1620) Interference coatings; (310.4165) Multilayer design.

References and links

1. J. Drevillon, K. Joulain, P. Ben-Abdallah, and E. Nefzaoui, "Far-field coherent thermal emission from a bilayer structure," J. Appl. Phys. **109**, 034315 (2011).
2. E. Nefzaoui, J. Drevillon, and K. Joulain, "Selective emitters design and optimization for thermophotovoltaic applications," J. Appl. Phys **111**, 084316 (2012).
3. E. Nefzaoui, J. Drevillon, Y. Ezzahri, and K. Joulain, "Simple far-field radiative thermal rectifier using Fabry-Pérot cavities based infrared selective emitters," Appl. Opt. **53**, 3479–3485 (2014).
4. I. Celanovic, D. Perreault, and J. Kassakian, "Resonant-cavity enhanced thermal emission," Phys. Rev. B **72**, 075127 (2005).
5. Y. Tsurimaki, P. O. Chapuis, R. Vaillon, J. Okajima, A. Komiya, and S. Murayama, "Reducing thermal radiation between parallel plates in the far-to-near field transition regime," in "Proceedings of the 15th International Heat Transfer Conference, Kyoto, Japan," (Aug. 10-15, 2014).
6. E. Blandre, P. O. Chapuis, M. Francoeur, and R. Vaillon, "Spatial and spectral distributions of thermal radiation emitted by a semi-infinite body and absorbed by a flat film," AIP Adv. **5**, 057106 (2015).
7. L. P. Wang, B. J. Lee, X. J. Wang, and Z. M. Zhang, "Spatial and temporal coherence of thermal radiation in asymmetric Fabry-Pérot resonance cavities," Int. J. Heat Mass Transf. **52**, 3024–3031 (2009).
8. L. P. Wang, S. Basu, and Z. M. Zhang, "Direct measurement of thermal emission from a Fabry-Pérot cavity resonator," J. Heat Transf. **134**, 072701 (2012).

#253052 Received 4 Nov 2015; revised 10 Dec 2015; accepted 13 Dec 2015; published 6 Jan 2016

9. B. J. Lee and Z. M. Zhang, "Design and fabrication of planar multilayer structures with coherent thermal emission characteristics," J. Appl. Phys. **100**, 063529 (2006).
10. P. Hanzelka, T. Kralik, A. Maskova, V. Musilova, and J. Vyskocil, "Thermal radiative properties of a DLC coating," Cryogenics **48**, 455–457 (2008).
11. V. Musilova, T. Kralik, P. Hanzelka, and A. Srnka, "Effect of different treatments of copper surface on its total hemispherical absorptivity bellow 77 K," Cryogenics **47**, 257–261 (2007).
12. V. Musilova, P. Hanzelka, T. Kralik, and A. Srnka, "Low temperature radiative properties of materials used in cryogenics," Cryogenics **45**, 529–536 (2005).
13. S. M. Rytov, I. U. A. Kravtsov, and V. Tatarskii, *Principles of Statistical Radiophysics: Elements of random fields*, Principles of Statistical Radiophysics (Springer-Verlag, 1989).
14. D. Polder and M. Van Hove, "Theory of radiative heat transfer between closely spaced bodies," Phys. Rev. B **4**, 3303–3314 (1971).
15. M. Francoeur, M. P. Mengüç, and R. Vaillon, "Solution of near-field thermal radiation in one-dimensional layered media using dyadic Green's functions and the scattering matrix method," J. Quant. Spectrosc. Radiat. Transf. **110**, 2002–2018 (2009).
16. M. Francoeur, M. P. Mengüç, and R. Vaillon, "Spectral tuning of near-field radiative heat flux between two thin silicon carbide films," J. Phys. D: Appl. Phys. **43**, 075501 (2010).
17. J. Drevillon, "Design ab-initio de matériaux micro et nanostructurés pour l'émission thermique cohérente en champ proche et en champ lointain," Thesis, Université de Nantes (2007).
18. L. P. Wang, S. Basu, and Z. M. Zhang, "Direct and indirect methods for calculating thermal emission from layered structures with nonuniform temperatures," J. Heat Transf. **133**, 072701 (2011).
19. P. O. Chapuis, S. Volz, C. Henkel, K. Joulain, and J. J. Greffet, "Effects of spatial dispersion in near-field radiative heat transfer between two parallel metallic surfaces," Phys. Rev. B **77**, 035431 (2008).
20. K. Joulain, J. P. Mulet, F. Marquier, R. Carminati, and J. J. Greffet, "Surface electromagnetic waves thermally excited: Radiative heat transfer, coherence properties and Casimir forces revisited in the near field," Surf. Sci. Rep. **57**, 59–112 (2005).
21. F. Marquier, K. Joulain, J. Mulet, R. Carminati, and J. Greffet, "Engineering infrared emission properties of silicon in the near-field and the far-field," Opt. Commun. **237**, 379–388 (2004).
22. R. Bauer, A. Schmid, P. Pavone, and D. Strauch, "Electron-phonon coupling in the metallic elements al, au, na, and nb: A first-principles study," Phys. Rev. B **57**, 11276–11282 (1998).
23. A. G. Mathewson and H. P. Myers, "Optical absorption in aluminium and the effect of temperature," J. Phys. F **2**, 403 (1972).
24. C. J. Fu and Z. M. Zhang, "Nanoscale radiation heat transfer for silicon at different doping levels," Int. J. Heat Mass Transf. **49**, 1703–1718 (2006).
25. H. H. Li, "Refractive index of silicon and germanium and its wavelength and temperature derivatives," J. Phys. Chem. Ref. Data **9** (1980).
26. E. Hecht, *Optics 2nd edition* (Addison-Wesley, 1987).
27. M. Laroche, F. Marquier, R. Carminati, and J. J. Greffet, "Tailoring silicon radiative properties," Opt. Commun. **250**, 316–320 (2005).
28. S. Edalatpour and M. Francoeur, "Size effect on the emissivity of thin films," J. Quant. Spectrosc. Radiat. Transf. **118**, 75–85 (2013).
29. A. Bid, A. Bora, and A. K. Raychaudhuri, "Temperature dependence of the resistance of metallic nanowires of diameter $\geq$15 nm : Applicability of Bloch-Grüneisen theorem," Phys. Rev. B **74**, 035426 (2006).

1. Introduction

The control of radiation emitted by a body is a topic of large and growing interest, for instance for tailoring the spectral distribution of radiation emitted by thermal sources in order to improve the performances of thermophotovoltaic converters. In the recent years, numerous studies have been conducted in this frame using one-dimensional multilayered structures (or photonic crystals). Drevillon et al. [1] showed that the resonances in the dielectric functions of semiconductors can be used to tailor sharp-peaked spectra of bilayer emitters. By considering more than two layers, Nefzaoui et al. [2] had to use a particle swarm algorithm to design multilayered emitters of at least two layers. In particular, they noticed that in the case of quadrilayer emitters with selected film thicknesses, the emissivity can exhibit a resonant behavior, due to interferences inside the cavities set by the interfaces of the system. For another purpose, i.e. thermal rectification between two planar bodies, the same group showed how interference phenomena inside multilayered emitters can be used [3]. In a more general frame, Celanovic et

#253052 Received 4 Nov 2015; revised 10 Dec 2015; accepted 13 Dec 2015; published 6 Jan 2016

al. [4] studied the emissivity of a simple structure composed of a Fabry-Pérot layer deposited on a substrate. They highlighted the increase of the spectral power of the emitter when interferences occur inside the layer. Interferences of thermal radiation can also be observed in the near-to-far field transition regime [5]. In this regime, the radiative heat flux exchanged by two semi-infinite planar bodies can be reduced because of destructive interferences. Going back to the thermophotovoltaics application, it was shown that for a semi-infinite radiator placed in the vicinity of a flat film, representing the photovoltaic converter [6] the frustrated modes, i.e. propagative in the emitter and evanescent in the vacuum gap separating the two bodies, can generate propagating modes that interfere in the film, thus possibly increasing absorption in it. As for experimental studies, measurements of the spectral reflectance of a structure consisting of a resonant layer sandwiched between two metallic layers actually exhibit peaks due to interference phenomena [7–9]. As for the temperature dependence of emissivity for bulk materials, which must be taken into consideration in such analyses, they were experimentally investigated for diamond-like-carbon [10], copper surfaces [11] and several other materials in cryogenic conditions [12].

In this article, after introducing briefly the physical and numerical modeling, we present a detailed analysis of the interference phenomena taking place inside an emitting layer acting as a Fabry-Pérot resonator in order to determine at which frequencies interferences occur. Then we investigate how those phenomena affect the total hemispherical emissivity of few-layer structures as a function of temperature, especially for structures composed of a resonant layer deposited on a reflective substrate. We highlight the existence of an optimal thickness of the resonant layer that maximizes the emissivity, and underline the role played by the variations of the dielectric function of the metallic substrate on the temperature-dependent total hemispherical emissivity. In the last section, we introduce ways to enhance those effects using additional layers. A metallic thin layer increases multireflections and therefore interferences. In particular, we observe that metallic thin layers have a high emissivity and are the main source of emission in the structure. Eventually, it is shown that for a given temperature, the addition of a second resonant layer enhances interference effects even more, and an optimal architecture that maximizes the emissivity of the structure under consideration is determined.

2. Methodology for the calculation of thermal radiation emission from the considered structures

In order to take wave effects such as interferences into account, we use the Fluctuational Electrodynamics approach [13] for computing the emissivities of selected structures. Maxwell's equations are solved to determine Green's tensors (that provide the link between the electromagnetic excitation of a medium with the response of another medium) while including the Fluctuation-Dissipation Theorem (that gives the stochastic currents generated by the electrical charges due to thermal motion in the source medium) [14, 15]. When the electric and magnetic fields are known, the calculation of the time-averaged Poynting vector provides the monochromatic radiative heat flux at a given location. The monochromatic radiative heat flux emitted by a source layer s can thus be written as [16]

$$q_\omega = \frac{k_0^2 \Theta(\omega,T)}{\pi^2} Re\left\{ i\epsilon_s^{"}(\omega) \int_0^{k_0} k_\rho dk_\rho \int_{z_s}^{z_s+1} \begin{pmatrix} g^E_{\rho\rho}(k_\rho,z',\omega) g^{H^*}_{\theta\rho}(k_\rho,z',\omega) \\ +g^E_{\rho z}(k_\rho,z',\omega) g^{H^*}_{\theta z}(k_\rho,z',\omega) \\ -g^E_{\theta\theta}(k_\rho,z',\omega) g^{H^*}_{\rho\theta}(k_\rho,z',\omega) \end{pmatrix} dz' \right\}, \quad (1)$$

where k_0 is the magnitude of the wavevector in vacuum, k_ρ is its component parallel to the interface, $\epsilon_s^{"}$ is the imaginary part of the dielectric function of the emitting layer, $\Theta(\omega,T)$ is the mean energy of a Planck oscillator, and $g^{E,H}_{\alpha\beta}$ are the Weyl components of the electric/magnetic

#253052 Received 4 Nov 2015; revised 10 Dec 2015; accepted 13 Dec 2015; published 6 Jan 2016

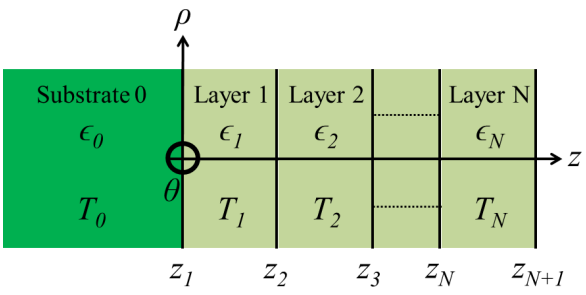

Fig. 1: Schematic representation of the one-dimensional system under consideration. Each layer l is characterized by its dielectric function ϵ_l, its temperature T_l and its boundaries z_l and z_{l+1}.

Green tensors, that are determined using a scattering matrix (S-matrix) approach [15, 17] so as to include the presence of other layers and possibly a substrate. The subscripts ρ, θ and z are related to the three orthogonal components in the cylindrical coordinate system, as depicted in Fig. 1. The integral over k_ρ physically means a summation over all the directions. The integral over z' is the summation over all the distributed source points of the emitting layer along the z direction, and is performed between its boundaries z_s and z_{s+1}. If a structure constituted of several layers is considered, the total heat flux emitted by this structure is the summation of the heat fluxes emitted by each layer. This approach allows separating and analyzing the contribution of each layer to the emission. We underline that in contrast to many works this method does not rely on Kirchhoff's law: we do not compute the reflectivity to determine the hemispherical emissivity. However, a previous work [18] emphasized the equivalence of the two methods: both of them allow considering temperature profiles in the emitting layers when the multilayer structure is not at equilibrium. In the following, we restrict ourselves to the equilibrium case.

Once the radiative heat flux is calculated, we can compute the hemispherical emissivity of the structure by dividing the radiative heat flux emitted by the structure - assumed to be at thermal equilibrium with a prescribed temperature - by the radiative heat flux emitted by a blackbody at the same temperature. Since the monochromatic heat flux emitted by a blackbody is given by:

$$q_\omega^{bb} = \Theta(\omega, T)\frac{k_0^2}{4\pi^2}, \tag{2}$$

the spectral hemispherical emissivity of an emitting layer of the structure taking into account the presence of other layers can be written as:

$$\varepsilon_\omega = 4Re\left\{ i\epsilon_s''(\omega)\int_0^{k_0} k_\rho dk_\rho \int_{z_s}^{z_s+1} \begin{pmatrix} g^E_{\rho\rho}(k_\rho,z',\omega)g^{H^*}_{\theta\rho}(k_\rho,z',\omega) \\ +g^E_{\rho z}(k_\rho,z',\omega)g^{H^*}_{\theta z}(k_\rho,z',\omega) \\ -g^E_{\theta\theta}(k_\rho,z',\omega)g^{H^*}_{\rho\theta}(k_\rho,z',\omega) \end{pmatrix} dz' \right\}. \tag{3}$$

The integration over all frequencies of the spectral radiative heat flux (Eq. (1)) results in the total hemispherical radiative heat flux emitted by the layer q^{tot}. Eventually, the total hemispherical emissivity of the layer can be obtained by dividing the total hemispherical radiative heat flux of the layer by the total hemispherical radiative heat flux of a blackbody at the same temperature, given by Stefan-Boltzmann's law:

#253052 Received 4 Nov 2015; revised 10 Dec 2015; accepted 13 Dec 2015; published 6 Jan 2016

$$\varepsilon = \frac{q^{tot}}{q^{bb}} = \frac{q^{tot}}{\sigma T^4}, \tag{4}$$

where σ is Stefan's constant. For simple systems, we can calculate analytically the Weyl components of the Green tensors. In the following, we will give the example of the spectral hemispherical emissivity of a substrate and of a thin layer deposited on a substrate. The spectral hemispherical emissivity of a single substrate in the absence of any other layer can be written as:

$$\varepsilon_\omega^{\text{Al substrate alone}} = \frac{1}{k_0^2}\int_0^{k_0} k_\rho dk_\rho \sum_{\gamma=s,p}(1-|r_{10}|^2), \tag{5}$$

where s and p are respectively the transverse electric and the transverse magnetic polarizations, and r_{10} is the reflection coefficient of the Al-vacuum interface. To calculate the spectral hemispherical emissivity of a Si monolayer deposited on an Al substrate, we have to calculate the emission of the Al substrate in presence of the Si layer, and the emission of the Si layer in the presence of the Al substrate. The spectral hemispherical emissivity associated to the Al substrate taking into account the presence of the Si layer is given by:

$$\varepsilon_\omega^{\text{Al substrate}} = \frac{1}{k_0^2}\int_0^{k_0} k_\rho dk_\rho \sum_{\gamma=s,p}\frac{(1-|r_{10}^\gamma|^2)(1-|r_{12}^\gamma|^2)}{|1-r_{10}^\gamma r_{12}^\gamma e^{2ik_{z1}t_1}|^2}, \tag{6}$$

where r_{10} and r_{12} are the Fresnel reflection coefficients of the Si-Al and the Si-vacuum interfaces, respectively. k_{z1} is the component of the wavevector perpendicular to the interface in the Si layer. Taking into account the presence of the Al substrate, the spectral hemispherical emissivity of the Si film is:

$$\varepsilon_\omega^{\text{Si layer}} = \frac{1}{k_0^2}\int_0^{k_0} k_\rho dk_\rho \sum_{\gamma=s,p}(1-|R_1^\gamma|^2-|T_1^\gamma|^2), \tag{7}$$

where R_1 and T_1 are the reflection and transmission coefficients of the Si film, and are functions of the Fresnel reflection and transmission coefficients:

$$R_1^\gamma = \frac{r_{01}+r_{12}e^{2ik_{z1}t_1}}{1+r_{01}r_{12}e^{2ik_{z1}t_1}}, \tag{8}$$

$$T_1^\gamma = \frac{t_{01}+t_{12}e^{2ik_{z1}t_1}}{1+r_{01}r_{12}e^{2ik_{z1}t_1}}. \tag{9}$$

Note that the terms $1+r_{01}^\gamma r_{12}^\gamma e^{2ik_{z1}t}$ are characteristic of a Fabry-Pérot cavity, i.e. they stand for multireflections between two interfaces. Eventually, the total hemispherical emissivity of the structure is the sum $\varepsilon_\omega^{\text{Al substrate}} + \varepsilon_\omega^{\text{Si layer}}$.

For the sake of simplicity, only two materials are investigated in this paper: silicon and aluminum, keeping in mind that the same principles and analysis could apply to similar materials. Aluminum is a metal, and will therefore act as a reflector inside the emitting structures. Its optical properties are well described by a Drude model [19, 20]:

$$\epsilon(\omega) = 1 - \frac{\omega_p^2}{\omega(\omega+i\Gamma)}, \tag{10}$$

where ω_p is the plasma frequency and Γ is the damping constant. To take into account the variations of the dielectric function of aluminum as a function of the temperature, the

#253052 Received 4 Nov 2015; revised 10 Dec 2015; accepted 13 Dec 2015; published 6 Jan 2016

temperature-dependent Drude parameters ω_p and Γ are calculated. The plasma frequency can be written as:

$$\omega_p^2 = \frac{Ne^2}{m^* \epsilon_0}, \tag{11}$$

where N is the density of electrons in aluminum, ϵ_0 is the dielectric permittivity of vacuum, m^* is the optical effective mass of the electron, and e its electrical charge. The damping constant can be written as [21]:

$$\Gamma = \frac{Ne^2 \rho}{m^*}, \tag{12}$$

where ρ is the electrical resistivity. The physical parameters that depend on temperature are the optical mass m^* and the electrical resistivity ρ. The values of the electrical resistivity as a function of temperature can be found in [22], and the variations of the optical effective mass of the electron as a function of temperature are taken from [23]. Using these values, we can fully take into account the effect of temperature variations on the dielectric function of aluminum.

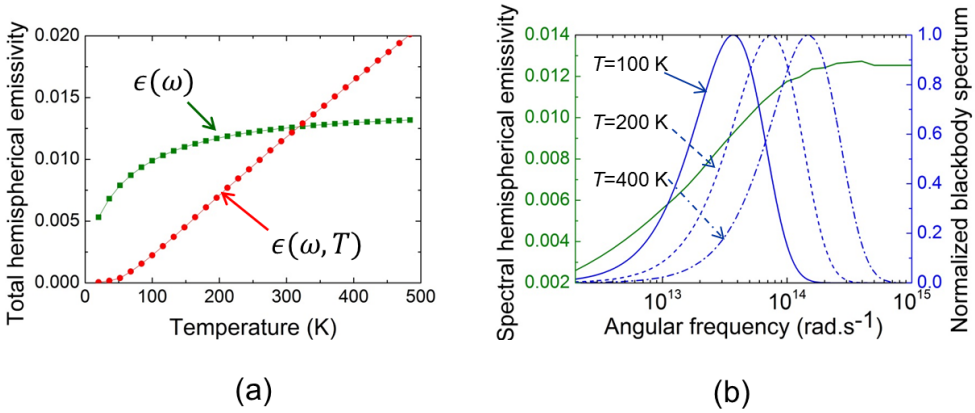

Fig. 2: (a): Total hemispherical emissivity of an aluminum susbtrate as a function of temperature. The green line represents the values calculated with the dielectric function of Al at ambient temperature. The red line represent the values calculated with the temperature-dependent dielectric function for Al. (b): Spectral hemispherical emissivity of an Al susbtrate at $T = 300$ K (green curve) and normalized blackbody spectra at different temperatures (blue curves).

We illustrate the importance of this effect in Fig. 2. In Fig. 2(a), the total hemispherical emissivity of a single Al substrate, calculated from Eq. (5), is plotted as a function of temperature. We compare the results when using the dielectric function of Al at ambient temperature, and when accounting for the variations of the dielectric function of Al as a function of temperature. We observe that the results are significantly different. When using a non-temperature dependent dielectric function, the variations of emissivity as a function of temperature are only due to the frequency shift of Planck's blackbody spectrum. When temperature increases, it shifts toward larger frequencies. It can be observed in Fig. 2(b) that the spectral emissivity of an Al substrate increases with the frequency. In reality, the dielectric function of Al is also modified when temperature varies. We observe that the dependence on temperature of the total hemispherical emissivity becomes proportional to the electrical resistivity of Al. As the electrical

#253052 Received 4 Nov 2015; revised 10 Dec 2015; accepted 13 Dec 2015; published 6 Jan 2016

Table 1: Resonance conditions for a single Si layer and a Si layer deposited on an Al substrate.

	$m=1$	$m=2$	$m=3$	$m=4$
Si layer alone	$\lambda_n = 2t$	$\lambda_n = t$	$\lambda_n = \frac{2t}{3}$	$\lambda_n = \frac{t}{2}$
Si layer on Al substrate	$\lambda_n = 4t$	$\lambda_n = \frac{4t}{3}$	$\lambda_n = \frac{4t}{5}$	$\lambda_n = \frac{4t}{7}$

resistivity varies proportionally to temperature, a rise of temperature induces an increase of the damping coefficient, leading to an increase of the spectral and total hemispherical emissivities. Accounting for the variations of the dielectric function of Al due to temperature is therefore crucial to study the temperature dependence of the emissivity of metallic emitters. Intrinsic silicon, or weakly doped silicon, has a constant refractive index in the infrared, and is almost lossless; it neither absorbs significantly. Thus, it is a good material for building Fabry-Pérot layers, because waves can be multireflected inside this material, thus maximizing interference effects. Its dielectric function is also calculated with a Drude model, whose parameters are doping dependent [21, 24]. Pure intrinsic silicon is difficult to obtain because there is always a residual doping. Therefore, we consider weakly doped silicon (with 10^{14} dopants per cm^{-3}) with a corresponding dielectric function close to pure intrinsic silicon. Silicon thin layers are almost non-emitting due to their high transparency in the infrared. Moreover, variations of the refractive index of silicon with temperature are weak [25], and thus are not taken into account in this article.

3. Determination of interference peaks in the spectral hemispherical emissivity of thin emitting films

Interferences occur when the size of a layer is of the same order of magnitude as the wavelength of the radiation inside this layer. Multireflections of waves with the same phase produce constructive interferences, while waves in phase opposition produce destructives interferences. The analysis of the phase lag due to the optical path difference between two waves that have been multireflected leads to the following resonance conditions for constructive interferences [26]:

$$\lambda_n(\omega) = \frac{2t\cos\varphi}{(m - \frac{\phi}{2\pi})}, \tag{13}$$

where $\lambda_n = \frac{\lambda}{n}$ denotes the wavelength of radiation inside the layer of refractive index n, t is the thickness of the layer, φ is the angle of incidence of the waves inside the layer and m is an integer, and λ is the wavelength of radiation in vacuum. The term ϕ corresponds to the phase lag due to the reflections, and is the sum of the arguments of the reflection coefficients of the two interfaces limiting the layer. To illustrate this formula, let us take the example of simple structures: a thin Si layer alone and a thin Si layer deposited on an Al substrate. Resonance conditions for both structures are reported in Table 1, considering only normal modes ($\varphi = 0$). We recall that the emission of such structures is quasi-isotropic, as shown in [2]. Therefore, an analysis of the normal modes can describe accurately the spectral behavior of interferences.

In Fig. 3, the spectral hemispherical emissivity of a single Si layer of thickness $t = 100$ μm (bottom left) and the same Si layer on an Al substrate (bottom right) are plotted. We observe the appearance of interference peaks, that strongly affect the spectral hemispherical emissivity of the emitter. On top, we show the evolution of the wavelength inside the Si layer λ_n as a function of angular frequency ω. The different conditions on λ_n for resonances given in Table 1 are represented by dashed horizontal lines. When a horizontal line crosses the curve $\lambda_n(\omega)$, resonance conditions are fulfilled. At those frequencies, we observe the appearance of interfer-

#253052 Received 4 Nov 2015; revised 10 Dec 2015; accepted 13 Dec 2015; published 6 Jan 2016

ence peaks (see the vertical lines). This allows determining at which frequencies interferences have an impact on the spectrum of thermal radiation emitted by thin films.

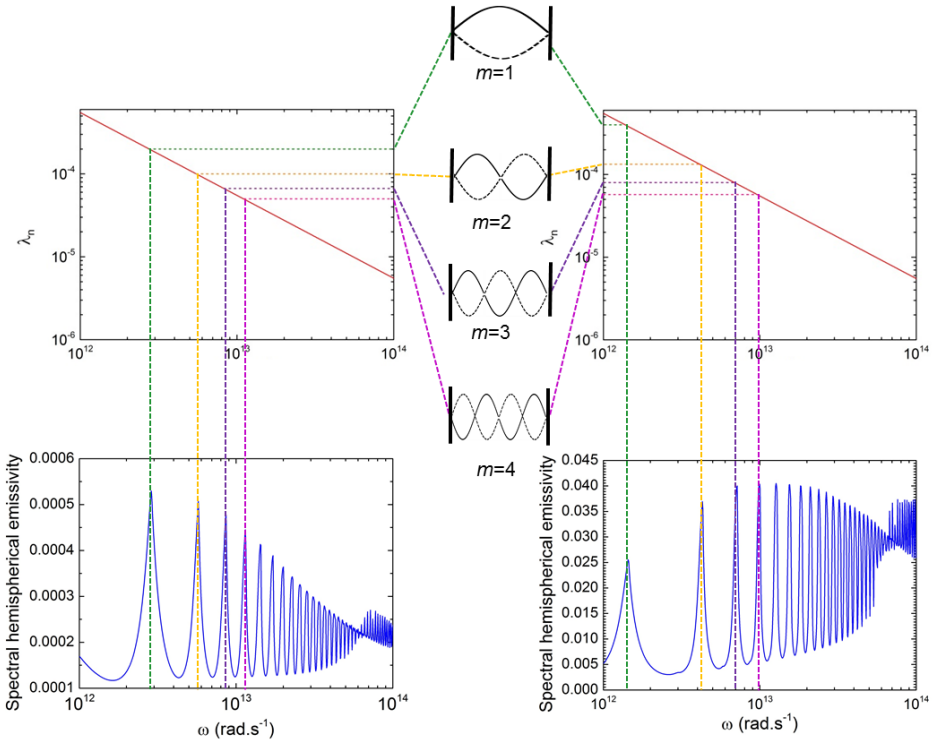

Fig. 3: Top left and right: wavelength inside the Si layer λ_n as a function of ω. Bottom left: spectral hemispherical emissivity of a single Si layer. Bottom right: spectral hemispherical emissivity of a Si layer on an Al substrate.

4. Temperature dependence of the total hemispherical emissivity of layered structures

In the previous section, we have mentioned that interferences in a resonant layer strongly affect the spectral hemispherical emissivity of the system over a large frequency range. Here, we are interested in analyzing the total hemispherical emissivity of layered structures and its dependence on temperature. When increasing the temperature of the system, the blackbody spectrum shifts to larger frequencies. The dependence on temperature of the hemispherical emissivity of the structure should be affected by interferences. To illustrate this phenomenon, the total hemispherical emissivity of a structure consisting of a Si monolayer of thickness t_1, acting as a Fabry-Pérot layer, and deposited on a reflective Al substrate is analyzed.

Figure 4 depicts the variations the total hemispherical emissivity of the structure as a function of the thickness of the Si layer for different temperatures. We compare the results when considering a temperature-independent dielectric function for Al at room temperature (Fig. 4(a)) and when accounting for the variations of the dielectric function of Al as a function of temperature (Fig. 4(b)). First, we observe that in both figures, the addition of a Si coating on an Al substrate increases the total hemispherical emissivity of the substrate alone (Fig. 2(a)), despite the fact that the Si layer is transparent and therefore non-emitting. The total hemispherical emissivity

#253052 Received 4 Nov 2015; revised 10 Dec 2015; accepted 13 Dec 2015; published 6 Jan 2016

exhibits several regimes: a plateau of low emissivity for low thicknesses, then a maximum at a given thickness that shifts toward lower thicknesses when the temperature increases, and a second plateau at larger thicknesses. If we now compare the results with and without the dependence on temperature of the dielectric function of Al, we observe that the optimal thickness that maximizes the emissivity at one temperature is the same for both cases. However, accounting for the variations of the Drude parameters of Al when the temperature increases leads to a significant increase of emissivity. The total hemispherical emissivity of the structures is thus strongly affected by the temperature-dependence of the optical properties of the emitting layer.

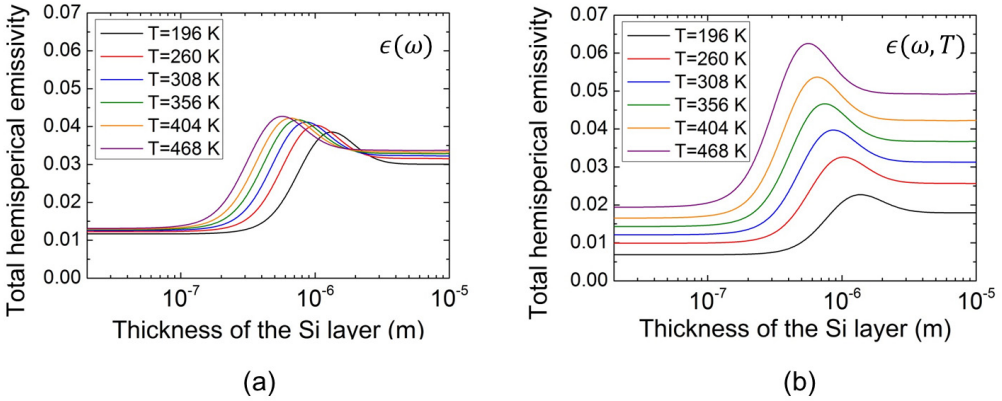

Fig. 4: Total hemispherical emissivity of a Si film coated on an Al substrate. (a): Considering the dielectric function of aluminum at room temperature. (b): Considering the temperature-dependent dielectric function of aluminum.

The optimal thickness t_{max} that maximizes the total hemispherical emissivity can be determined by analyzing the frequency of the first-order peak (smallest frequency) of interference and the frequency of the maximum intensity of Planck's blackbody spectrum at the considered temperature. At a temperature T, Planck's blackbody intensity is maximum at a frequency $\omega_{max} = C \times T$, according to Wien's law, where C is a constant equal to $3.6971 \times 10^{11} \mathrm{s}^{-1}\mathrm{K}^{-1}$ when Planck's distribution function is expressed in terms of angular frequency.

In Fig. 5, the spectral hemispherical emissivity of the structure under consideration (a Si film on an Al substrate) is plotted for different Si film thicknesses. The normalized Planck blackbody spectrum at $T = 300$ K is also plotted. For $t = 10$ nm (Fig. 5(a)), the Si film is too thin for interferences to occur in the spectral range where the blackbody spectrum at 300 K extends. Analyzing the denominator of Eq. (6) which includes the term that accounts for multireflections, we find that the argument of the exponential term is close to 0 when $t_1 << \frac{c}{n\omega_{max}}$ and interferences cannot occur at the considered temperature. When the thickness of the film reaches $t \sim \frac{c}{n\omega_{max}}$, the first peak of interference in the spectral hemispherical emissivity starts to overlap the Planck blackbody spectrum (Fig. 5(b)), and the total hemispherical emissivity of the structure increases. At the thickness where the total hemispherical emissivity is maximum, the first peak of interference is close to the frequency ω_{max} (Fig. 5(c)). For each temperature, the ratio between the frequency ω_{max} and the frequency of the first-order peak of interference ω_{fp} was numerically found to have almost the same value ($\frac{\omega_{max}}{\omega_{fp}} \sim 0.72$ - 0.74). When the thickness of the film increases even more, a larger number of interfering modes overlap the blackbody spectrum (Fig. 5(d)), and the total hemispherical emissivity reaches a plateau. In

#253052 Received 4 Nov 2015; revised 10 Dec 2015; accepted 13 Dec 2015; published 6 Jan 2016

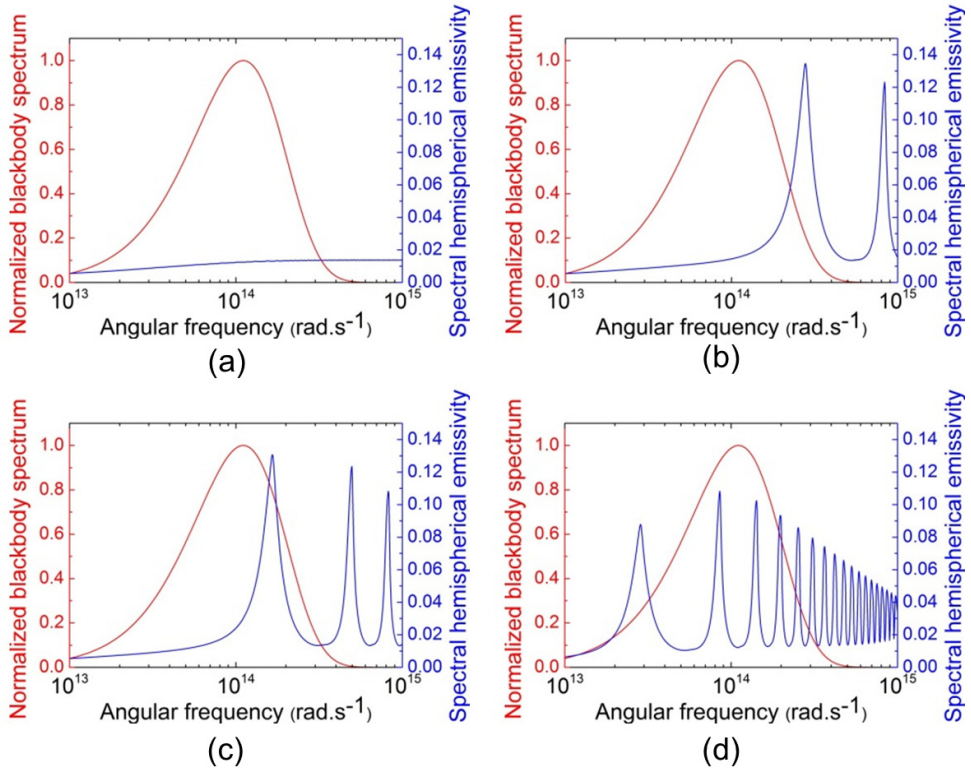

Fig. 5: Spectral hemispherical emissivity of the structures (blue lines) and blackbody spectrum at $T = 300$ K for different thicknesses of the Si layer. (a): $t = 10$ nm (b): $t = 500$ nm (c): $t = 874$ nm (d): t=5 μm.

Eq. (6), we can observe that when t becomes much larger than $\frac{c}{n\omega_{max}}$, the factor that accounts for multireflections in the Fabry-Pérot layer reduces to 1 meaning a lot of multireflections occur in the spectral range where the blackbody extends, leading to a constant value of the total hemispherical emissivity.

We now focus on the temperature dependence of the emissivity of the structures under consideration. Total hemispherical emissivities of the Si monolayer on the Al substrate are plotted as a function of temperature in Fig. 6(a) for different Si layer thicknesses. Total hemispherical emissivities increase with temperature, but at different rates when considering different layer thicknesses. Again, this increase is due to two separated effects: the frequency shift of the blackbody spectrum and the variations of the optical properties of Al when temperature varies. To separate the two effects, we define the enhancement factor of a given structure as the total hemispherical emissivity of the structure divided by the total hemispherical emissivity of a single Al substrate at a given temperature. By doing this, we can analyze the impact of the frequency shift of the blackbody spectrum without the impact of the variations of the optical properties of Al when temperature increases. In Fig. 6(b), we plot the enhancement factor as a function of temperature for different layer thicknesses. For each thickness, the enhancement factor reaches a maximum at a given temperature, close to 3.3. Like previously, this temperature can be related to the spectral position of the maximum intensity of Planck's blackbody

#253052 Received 4 Nov 2015; revised 10 Dec 2015; accepted 13 Dec 2015; published 6 Jan 2016

spectrum and of the first peak of interference. Note that much larger enhancement factors can be reached with layer materials of larger refractive indices n (not shown here).

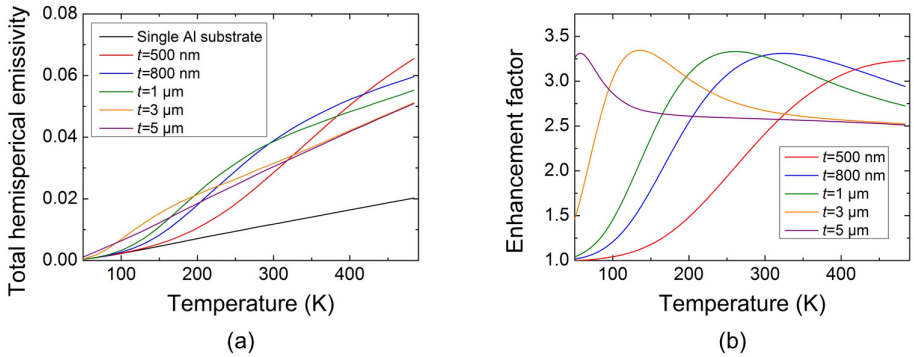

Fig. 6: (a): Total hemispherical emissivity of the Si monolayer on an Al substrate as a function of temperature for different Si layer thickesses. (b): Enhancement factor as a function of temperature for different thicknesses.

As a conclusion, interferences affect the total hemispherical emissivity of the structure and also its temperature dependence, and it is possible to determine the Si layer thickness that maximizes it for each temperature.

5. Enhancing interference effects with few-layer structures

In the previous sections, we have used a silicon layer coated on top of aluminum as the Fabry-Pérot layer. The two interfaces at the boundaries of the layer are not the same, and the Si-vacuum interface is less reflective than the Si-Al interface: this might not be the optimal configuration for having a maximum impact of interferences. In addition, the hemispherical emissivities calculated in the previous sections are overall quite low, because silicon is transparent in the frequency range of interest for the temperature considered, and aluminum is highly reflective. In this section, we show that we can tune and exalt the effects described before with few-layer structures, as depicted in Fig. 7.

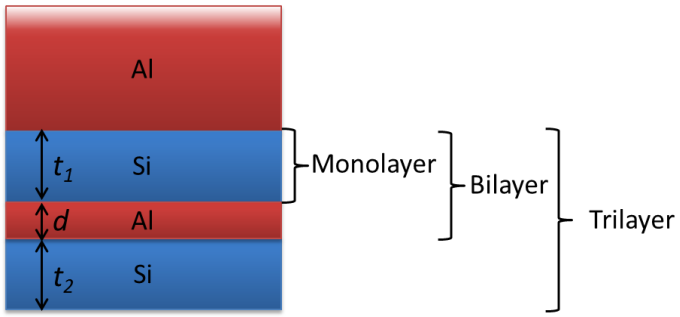

Fig. 7: Schematic representation of the investigated structures.

To enhance interference effects, a thin aluminum layer is first added onto the silicon layer

#253052 Received 4 Nov 2015; revised 10 Dec 2015; accepted 13 Dec 2015; published 6 Jan 2016

to form an asymmetric Fabry-Pérot cavity [7–9], also referred to as Salisbury screen in the literature [27], and named here as a bilayer structure. The thickness of the metallic layer is critical: if the film is too thick, waves interfering in the Si layer will not be transmitted through the film. Furthermore, unlike semiconductors, hemispherical emissivity of metallic thin layers increases exponentially above a critical thickness. This effect was described in [28], where the threshold thickness was estimated to be a few dozens of nanometers. Using a thin metallic layer, it is possible to both increase hemispherical emissivity and enhance interferences effects in the Si layer. In the following, we keep using the bulk dielectric function for the nanometer-thin metallic layer. The actual values may depart from it due to spatial dispersion [19] and electron collision with boundaries [29], that are expected to increase the energy dissipation in the thin metallic layer.

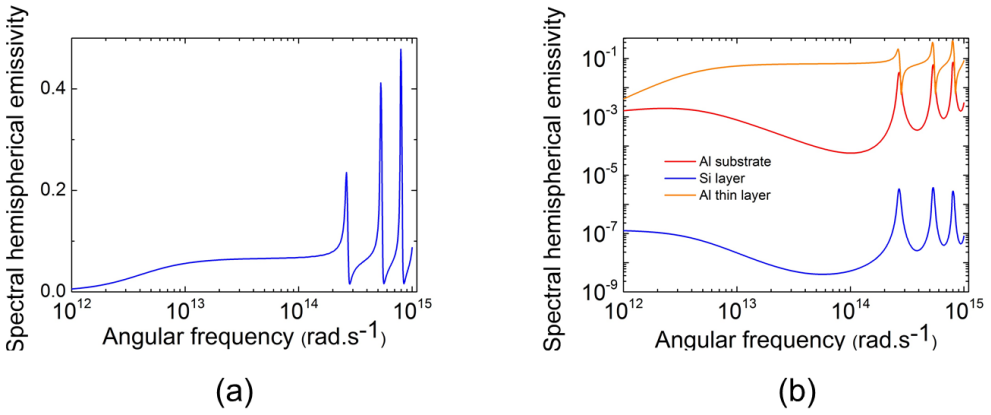

Fig. 8: (a) Spectral hemispherical emissivity of the bilayer structure on an Al substrate, for $t_1 = 1$ μm and $d = 5$ nm. (b) Participation of each layer to the hemispherical emissivity.

The spectral hemispherical emissivity of a bilayer structure on an Al substrate, made of a 1 μm thick silicon layer and a thin aluminum layer of thickness 5 nm, is reported in Fig. 8(a). It is observed that interferences have a larger amplitude, and also that the overall hemispherical emissivity of the structure is larger than the hemispherical emissivity of the monolayer. One can notice that the shape of the interference peaks is now asymmetric. Furthermore, the spectral hemispherical emissivity of the structure reaches a minimum right after the maximum. An explanation of this phenomenon can be found in [7], where the analytical function of the reflectance of the structure was analyzed. Participation of each layer to the hemispherical emissivity of the structure is plotted in Fig. 8(b). It is worth noticing that most of the emission, as well as the asymmetric shape of the interference peaks, come from the thin aluminum layer. In summary, the Al thin layer is the main source of emission in this structure, and waves emitted by this film are interfering inside the Si layer. This structure exhibits therefore larger values of spectral hemispherical emissivity, and interference peaks with larger amplitudes.

Finally, a second silicon layer is added onto the aluminum thin film to build a trilayer structure. We report in Fig. 9(a) the total hemispherical emissivity of the structure as a function of the thicknesses t_1 and t_2 of the two Si layers. For a given thickness t_1, there is a thickness t_2 that maximizes the total hemispherical emissivity of the structure, and vice versa. The maximum of total hemispherical emissivity of the structure corresponds to the intersection of the optimal thicknesses for both t_1 and t_2. On Fig. 9(a), the horizontal dashed line represents the thickness

#253052 Received 4 Nov 2015; revised 10 Dec 2015; accepted 13 Dec 2015; published 6 Jan 2016

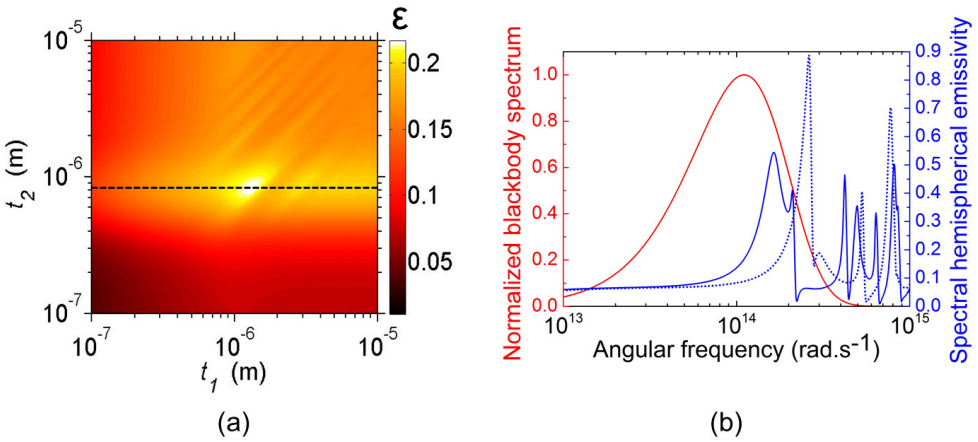

Fig. 9: (a): Total hemispherical emissivity of a trilayer structure at $T = 300$ K and $d = 5$ nm as a function of t_1 and t_2. The horizontal dashed line represents the thickness that maximizes the emissivity of the monolayer structure at the same temperature. (b): Spectral hemispherical emissivity for $t_1 = 1$ µm and $t_2 = 0.5$ µm (conditions fullfilling Eq. (14); blue dotted line), and for the structure maximizing the total hemispherical emissivity (plain blue line). The blackbody spectrum at 300 K is superimposed.

that maximizes the total hemispherical emissivity of the monolayer structure at the same temperature. We observe that the optimal thickness t_1 is very close to this value, which is consistent after noticing that the second layer of thickness t_2 of the trilayer structure is equivalent to the layer of the monolayer structure in terms of interfaces, and therefore of resonance conditions. It can indeed be expected that the maximum of the total hemispherical emissivity of the structure corresponds to the case where the first-order peaks of interference for both cavities occur at the same frequency, to form a large peak of emission as described in [2]. Using Eq. (13) for both cavities gives:

$$\lambda_n = \frac{2t_1 \cos\varphi}{(m - \frac{\phi_1}{2\pi})} = \frac{2t_2 \cos\varphi}{(m - \frac{\phi_2}{2\pi})}, \tag{14}$$

where ϕ_1 and ϕ_2 are the phase lags due to reflections at the interfaces at the boundaries of the layers, that take a value close to 0 and π respectively. Using this expression for $m = 1$, the first peak of interference in each layer overlaps when the thickness of the first layer t_1 is twice larger than the thickness of the second layer t_2, as depicted in Fig. 9(b) (dotted line). In this case, the spectral hemispherical emissivity exhibits a large peak, that reaches a value close to 0.9. But according to Fig. 9(a), this is not the configuration that maximizes the total hemispherical emissivity of the structure. In fact, the maximum of emissivity occurs when the first-order peaks of interference of both layers do not occur at the exact same frequency, but still overlap with the envelope of the blackbody at the considered temperature, as depicted in Fig. 9(b) (full blue line), where the spectral hemispherical emissivity of the structure with the optimal architecture is plotted.

The addition of a second Fabry-Pérot layer can therefore enhance the emissivity even more, and the successive addition of layers on the aluminum substrate increases the total hemispherical emissivity of the structure by one order of magnitude when using the optimal parameters of

#253052 Received 4 Nov 2015; revised 10 Dec 2015; accepted 13 Dec 2015; published 6 Jan 2016

Table 2: Maximum values of the spectral and total hemispherical emissivities at $T = 300$ K for each structure. The values for a simple Al substrate and a single Al thin layer are given for comparison.

	Al substrate	Al thin layer	Monolayer	Bilayer	Trilayer
Spectral maxima	0.01	0.06	0.13	0.48	0.89
Total maxima	0.01	0.06	0.03	0.07	0.21

the system, as shown in Table 2.

6. Conclusion

The influence of interferences on the spectral hemispherical emissivity and on the total hemispherical emissivity of layered structures as a function of temperature has been investigated. We have highlighted the impact of the variations with temperature of the optical properties of metallic layers on the hemispherical emissivity. We have shown that when interferences occur in an emitting layer, the spectral hemispherical emissivity of the structure exhibits sharp peaks, whose frequencies depend on the size of the layer and its refractive index. Hemispherical emissivities are increased, and an optimal film thickness that maximizes the hemispherical emissivity has been highlighted. We have also investigated how multilayered structures can enhance these effects, using an additional thin metallic film and a second layer to enhance interference effects. In the end, we are able to increase the total hemispherical emissivity by a factor 20 in comparison to the bulk, and by a factor 6 in comparison to the thin metallic film. With the understanding of these phenomena, we have demonstrated that it is possible to provide a method with physical bases for maximizing the total hemispherical emissivity of few-layer structures. Thus, this work paves the way for new optimizations in several applications, such as those which require controlling the total radiative heat transfer between two bodies (for instance radiative rectification and radiative cooling) or tuning the spectrum of the radiative heat flux, for instance for thermophotovoltaics.

Acknowledgments

The authors would like to acknowledge Mathieu Francoeur for longstanding collaboration and his support on the numerical calculations.

#253052 Received 4 Nov 2015; revised 10 Dec 2015; accepted 13 Dec 2015; published 6 Jan 2016